


Nonlinear non-Hermitian higher-order topological laser

Motohiko Ezawa 

Department of Applied Physics, University of Tokyo, Hongo 7-3-1, 113-8656, Japan



(Received 10 December 2021; accepted 16 February 2022; published 11 March 2022)

Topological lasers are investigated in nonlinear, non-Hermitian, and topological lattice systems based on a quench dynamics starting from one site. Explicitly, we consider the topological laser in the Su-Schrieffer-Heeger model with two topological edge states and the second-order topological laser in the breathing kagome lattice with three topological corner states. Once we stimulate any one site, after some delay, all sites belonging to the topological edge or corner states are shown to emit stable laser light depending on the density of states, although no wave propagation is observed from the stimulated site. Thus the profile of topological edge or corner states is observable by measuring the intensity of lasing. The phenomenon occurs due to a combinational effect of linear non-Hermitian loss terms and nonlinear non-Hermitian gain terms in the presence of the topological edge or corner states. It is intriguing that the dynamics of topological edge or corner states are observed in real-time and real-space dynamics of the laser emission.

DOI: [10.1103/PhysRevResearch.4.013195](https://doi.org/10.1103/PhysRevResearch.4.013195)

I. INTRODUCTION

Topological physics is one of the most essential concepts found in recent fundamental physics [1,2]. Recently, it is ubiquitously found in various systems in photonic [3–22], acoustic [23–32], mechanical [33–37], and electric circuit [38–45] systems. Among them, topological photonics is most extensively studied theoretically and experimentally. One of the reasons is that it is possible to observe real-time and real-space dynamics. Another merit is that topological photonics has opened a new field of topological physics, i.e., non-Hermitian topology, nonlinear topology, and their combination. Non-Hermitian effects are introduced by a loss and a gain of photons. On the other hand, nonlinear effects are introduced by the Kerr effect or a stimulated emission effect.

A topological laser is a prominent application of topological physics [12,13,46–54]. It utilizes topological edge states for the coherent laser emission. Thanks to the topological protection, the topological laser is robust against the randomness and the defects of the sample, which is favorable for future laser applications. A topological laser is an ideal playground to investigate nonlinear non-Hermitian topological physics. The loss of photons and gain from stimulated emissions constitute the non-Hermitian terms. The nonlinear effect is included in the gain term, which represents the saturation of the gain.

Higher-order topological phases are an extension of topological phases [55–62]. There emerge topological corner states in the second-order topological phase. One of the simplest examples is given by the breathing kagome lattice, where

three topological corner states appear in triangle geometry. This model is a natural generalization of the Su-Schrieffer-Heeger (SSH) model to two dimensions. Since the model requires only positive hoppings, it is realized in various systems including photonic [17,19], acoustic [29,30], and electric circuit systems [63].

In this paper, we analyze a quench dynamics of a nonlinear non-Hermitian topological laser and a higher-order topological laser by stimulating any one site. We study explicitly the SSH model for a topological laser and the breathing kagome model for a higher-order topological laser. In the SSH model with two topological edge states, once we stimulate any one site, after some delay, all sites belonging to the two topological edge states begin to emit stable laser light depending on the density of states (DOS), although no wave propagation is observed from the stimulated site. Thus the profile of a topological edge state together with the DOS is observable by laser intensity. The strength of the laser light is identical for the two edges because of reflection symmetry. This is also the case for the second-order topological laser in the breathing kagome lattice with three topological corner states. Here, the system has trigonal symmetry. The phenomenon occurs due to a combinational effect of linear non-Hermitian loss terms and nonlinear non-Hermitian gain terms in the presence of the topological edge or corner states. It is remarkable that the dynamics of topological edge or corner states are observed in real-time and real-space dynamics of the laser emission.

II. TOPOLOGICAL LASER

A. Model

We consider a coupled-ring system made of active resonators [46]. The dynamics of a laser system is governed by [46]

$$i \frac{d\psi_n}{dt} = \sum_{nm} M_{nm} \psi_m - i\gamma \left(1 - \xi \frac{P_n}{1 + |\psi_n|^2/\eta} \right) \psi_n, \quad (1)$$

Published by the American Physical Society under the terms of the Creative Commons Attribution 4.0 International license. Further distribution of this work must maintain attribution to the author(s) and the published article's title, journal citation, and DOI.

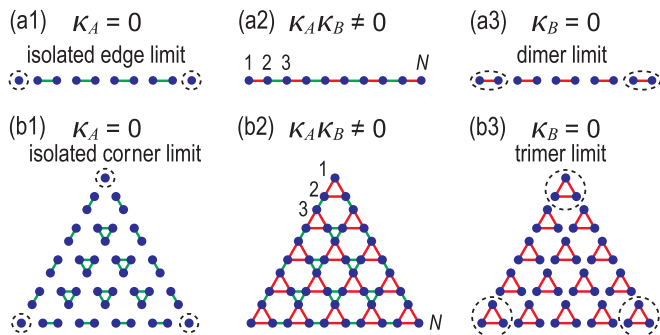


FIG. 1. (a1)–(a3) Illustration of a dimerized lattice with (a1) $\kappa_A = 0$, (a2) $\kappa_A \kappa_B \neq 0$, and (a3) $\kappa_B = 0$. (b1)–(b3) Illustration of a breathing kagome lattice with (b1) $\kappa_A = 0$, (b2) $\kappa_A \kappa_B \neq 0$, and (b3) $\kappa_B = 0$. A line (triangle) contains many small segments (triangles). At the edges (corners) of the chain (triangle), there are two (three) isolated atoms for $\kappa_A = 0$, while there are dimer (trimer) states for $\kappa_B = 0$. They are marked by dashed circles. Lattice sites are numbered from $n = 1$ to N as indicated in (a2) and (b2).

where ψ_n is the amplitudes of the site n , where $n = 1, 2, 3, \dots, N$ in the system composed of N sites; M_{nm} describes a hopping matrix; γ represents the loss in each resonator; $\gamma\xi$ represents the amplitude of the optical gain via stimulated emission; η represents the nonlinearity; and P_n stands for the spatial profile of the pump. The system turns into the linear model in the limit $\eta \rightarrow \infty$. On the other hand, γ controls the non-Hermiticity. The system turns into a Hermitian model for $\gamma = 0$. We call the term proportional to γ the loss term and the term proportional to $\gamma\xi$ the nonlinear gain term.

We take

$$P_n = \sum_{\bar{n}} \delta_{n,\bar{n}}, \quad (2)$$

where \bar{n} runs over the edge or corner sites. Namely, optical gains are introduced only at the edge or corner sites.

We are interested in the case where M_{nm} represents a tight-binding model possessing a topological phase. We explicitly consider the SSH model illustrated in Figs. 1(a1)–1(a3), where \bar{n} takes values at the left and right edges, and the breathing kagome model illustrated in Figs. 1(b1)–1(b3), where \bar{n} takes values at the top, bottom-left, and bottom-right corners.

It is possible to solve Eq. (1) numerically for explicit system parameters, as we do later. However, to reach a deeper understanding of the phenomena, an analytical study is indispensable. Since this is impossible for general system parameters, we make an analytical study for special cases.

B. Edge or corner dynamics

We first consider the dynamics of an edge or corner site when it is perfectly isolated as in Figs. 1(a1) or 1(b1). This is the case where $M_{nm} = 0$ for the edge or corner sites. For instance, this is realized by setting $\kappa_A = 0$ in Eq. (12) or $\lambda = -1$ in Eq. (15) for the SSH model.

The dynamics is governed by isolated equations,

$$\frac{d\psi_{\bar{n}}}{dt} = -\gamma \left(1 - \xi \frac{1}{1 + |\psi_{\bar{n}}|^2/\eta} \right) \psi_{\bar{n}}. \quad (3)$$

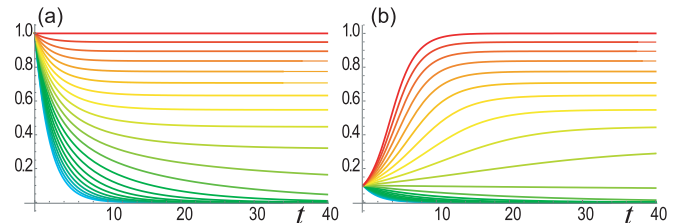


FIG. 2. Dynamics of the isolated equation (3) under the initial conditions (a) $\psi_1(0) = 1$ and (b) $\psi_1(0) = 0.1$. The solutions reach the same stationary solution irrespective of the initial conditions. Red color indicates the solution with $\xi = 2$, while cyan color indicates that with $\xi = 0$. We have set $\eta = 1$ and $\gamma = 1/2$.

Solving this equation numerically with two different initial conditions $\psi_{\bar{n}} = 1$ and $\psi_{\bar{n}} = 0.1$, we show the results in Figs. 2(a) and 2(b), respectively. It is intriguing that the dynamics of the topological edge or corner state does not depend on the initial condition of $\psi_{\bar{n}}$. The saturated value of $\psi_{\bar{n}}$ as $t \rightarrow \infty$ is identical for all isolated edge or corner states. This can be understood analytically as follows.

We solve Eq. (3) for nontrivial stationary solutions. The stationary solution for an edge or corner site \bar{n} is given by

$$\xi \frac{1}{1 + |\psi_{\bar{n}}|^2/\eta} = 1. \quad (4)$$

Hence the nontrivial solution reads

$$\lim_{t \rightarrow \infty} |\psi_{\bar{n}}|^2 = \eta(\xi - 1), \quad (5)$$

where it is necessary that $\xi > 1$.

As a result, there are only two stable solutions in Eq. (3). One is the ground-state mode $\psi_{\bar{n}} = 0$ for any value of ξ , and the other is the stimulated mode $|\psi_{\bar{n}}|^2 = \eta(\xi - 1)$ for $\xi > 1$. The initial condition determines which state is realized.

The nonlinear term is essential to have a nontrivial stationary solution. Indeed, we obtain a linear theory in the limit $\eta \rightarrow \infty$, where the amplitude $|\psi_n|^2$ diverges.

The state remains real for a real initial condition, and Eq. (3) is simplified to

$$\frac{d\psi}{-\psi_{\bar{n}} + \xi \frac{1}{1 + \psi_{\bar{n}}^2/\eta} \psi_{\bar{n}}} = \gamma dt, \quad (6)$$

which is solved as

$$\frac{2 \ln |\psi_{\bar{n}}| - \xi \ln [\gamma(\psi_{\bar{n}}^2/\eta + 1 - \xi)]}{2(\xi - 1)} = \gamma(t + t_0). \quad (7)$$

The state evolution $\psi_{\bar{n}}(t)$ is given by the inverse of this equation.

C. Bulk dynamics

We next analyze the dynamics of the bulk site, where there is no nonlinear non-Hermitian term because $P_n = 0$. Then, the dynamics is governed by the linear equation

$$i \frac{d\psi_n}{dt} = \sum_{nm} M_{nm} \psi_m - i\gamma \psi_n. \quad (8)$$

With the use of a solution of the linear equation

$$i \frac{d\psi_n^0}{dt} = \sum_{nm} M_{nm} \psi_m^0, \quad (9)$$

Eq. (8) is solved as

$$\psi_n = e^{-\gamma t} \psi_n^0. \quad (10)$$

This means that the amplitude exponentially decays as a function of time in the bulk.

D. Quench dynamics

To reveal the property of the system, we investigate the quench dynamics by giving a pulse to one site and exploring its time evolution subject to Eq. (1). This provides us with a good signal to detect whether the system is topological or trivial [64]. It has also been applied to various nonlinear systems to manifest the self-trapping phenomena intrinsic to the nonlinearity effect [65–68].

Let us study a quench dynamics starting from one site indexed by m ,

$$\psi_n(t) = \delta_{n,m} \quad \text{at } t = 0, \quad (11)$$

where $m = 1$ represents the left-edge site or the top-corner site as in Figs. 1(a2) and 1(b2). We solve Eq. (1) under the initial condition (11).

The quench dynamics describes a nonequilibrium dynamics. However, the point is that we just give a small signal only to one site. Its time evolution is like a small surface wave propagating over the sample by detecting its static property without disturbing it. Hence the quench dynamics well captures properties of the sample at equilibrium, including the topological property governed by the hopping matrix M_{nm} and the self-trapping effect due to the nonlinearity. In this sense, the quench dynamics method is analogous to the Green’s function method, where a test particle is injected into the system to detect properties of the system at equilibrium.

III. NONLINEAR NON-HERMITIAN SSH MODEL

A. Model

A topological laser based on the SSH model has been discussed [12,13,48–53]. We consider the case where the hopping matrix is governed by the SSH matrix in Eq. (1). The matrix is explicitly given by

$$M_{nm} = -(\kappa_A + \kappa_B)\delta_{n,m} + \kappa_A(\delta_{2n,2m-1} + \delta_{2m,2n-1}) + \kappa_B(\delta_{2n,2m+1} + \delta_{2m,2n+1}). \quad (12)$$

We show the band structure for a finite chain in Fig. 3(a2).

The explicit equations for a finite chain with length N are given by

$$i \frac{d\psi_{2n-1}}{dt} = \kappa_A(\psi_{2n} - \psi_{2n-1}) + \kappa_B(\psi_{2n-2} - \psi_{2n-1}) - i\gamma \left(1 - \xi \frac{\delta_{n,1}}{1 + |\psi_{2n-1}|^2/\eta} \right) \psi_{2n-1}, \quad (13)$$

$$i \frac{d\psi_{2n}}{dt} = \kappa_B(\psi_{2n+1} - \psi_{2n}) + \kappa_A(\psi_{2n-1} - \psi_{2n}) - i\gamma \left(1 - \xi \frac{\delta_{n,N}}{1 + |\psi_{2n}|^2/\eta} \right) \psi_{2n}. \quad (14)$$

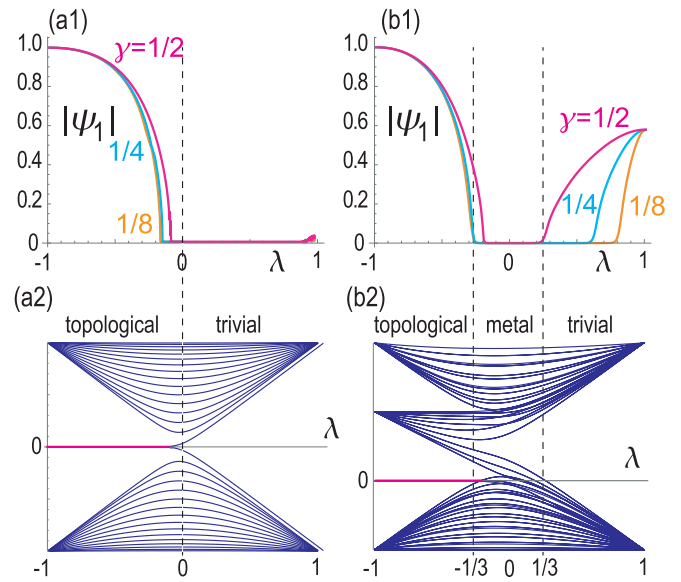


FIG. 3. Saturated amplitude $|\psi_1|$ at (a1) the edge site in the SSH model and (b1) the corner site in the breathing kagome model, where $\gamma = 1/2$ for magenta, $\gamma = 1/4$ for cyan, and $\gamma = 1/8$ for orange. (a2) The energy spectrum in the SSH model made of a finite chain with topological edge states in red for $\lambda < 0$. (b2) The energy spectrum of the breathing kagome model in triangle geometry with topological corner states in red for $\lambda < -1/3$. The horizontal axis is λ . We have set $\kappa = 1$, $\eta = 1$, and $\xi = 2$.

It is convenient to introduce the coupling strength κ and the dimerization parameter λ by

$$\kappa_A = \kappa(1 + \lambda), \quad \kappa_B = \kappa(1 - \lambda), \quad (15)$$

with $|\lambda| \leq 1$. The isolated edge limit is realized at $\lambda = -1$ in Fig. 1(a1).

B. Topological number in the SSH model

The present SSH model (1) has the same topological structure as in the original SSH model by the following reasoning. First, there is no contribution of the nonlinear gain term ($\propto \gamma\xi$) to the bulk since it exists only at the edge site. Next, the loss term ($\propto \gamma$) only shifts the matrix as

$$\bar{M}_{nm} \equiv M_{nm} - i\gamma\delta_{nm}. \quad (16)$$

Equation (1) is rewritten in the form of the linear model for the bulk ($n \neq \bar{n}$),

$$i \frac{d\psi_n}{dt} = \sum_{nm} \bar{M}_{nm} \psi_m. \quad (17)$$

Then, the topological properties are determined by the hopping matrix \bar{M}_{nm} .

The hopping matrix is explicitly given by

$$\bar{M}(k) = -(\kappa_A + \kappa_B + i\gamma)I_2 + M_0(k) \quad (18)$$

in the momentum space, with

$$q(k) = \kappa_A + \kappa_B e^{-ik} \quad (19)$$

and

$$M_0(k) = \begin{pmatrix} 0 & q(k) \\ q^*(k) & 0 \end{pmatrix}. \quad (20)$$

The topological number in the original SSH model is given by the Berry phase

$$\Gamma = \frac{1}{2\pi} \int_0^{2\pi} A(k) dk, \quad (21)$$

where $A(k) = -i\langle \phi(k) | \partial_k | \phi(k) \rangle$ is the Berry connection with $\phi(k)$ being the eigenfunction of $\bar{M}(k)$. Note that the diagonal term in Eq. (17) with Eq. (12) does not contribute to the topological charge because the wave function $\phi(k)$ does not depend on the diagonal term. Hence the present model (1) has the same phases as the original SSH model. The system is topological for $\lambda < 0$ with the emergence of the topological edge states marked in red, while it is trivial for $\lambda > 0$ as in Fig. 3(a2).

C. Quench dynamics

We numerically solve Eqs. (13) and (14) under the initial condition (11) by taking $m = 1$. We show the time evolution of $|\psi_n|$ in Fig. 4. The results of the quench dynamics are significantly different between the topological and trivial phases. In the topological phase, the amplitude $|\psi_1|$ at the left edge is rapidly saturated as shown by the red curve in Fig. 4(a2), while there is a delay in the saturation of the amplitude $|\psi_N|$ at the right edge as shown by the cyan curve in Fig. 4(a2). The delay implies the propagation of a wave along a chain, although the propagation of the wave is invisible in Fig. 4(a1), as is consistent with Eq. (10). This means that a wave with a tiny amplitude transfers the information of the excitation to the right edge and induces a stimulated emission. On the other hand, in the trivial phase, the amplitude $|\psi_1|$ rapidly decreases as shown in Fig. 4(a2). Furthermore, there is no excitation $|\psi_N|$ at the right edge.

Figure 4(a3) shows a spatial profile of the amplitude $|\psi_n|$ after enough time, which is the DOS for a pair of topological edge states in nonlinear non-Hermitian system.

We find that there is no reflection of the propagating wave by the right edge. This is due to the loss term ($\propto \gamma$) in the bulk. It is highly contrasted with the case of the Hermitian model. In addition, the amplitudes $|\psi_1|$ and $|\psi_N|$ are always identical. This is due to reflection symmetry $x \longleftrightarrow N - x$ on the right-hand side of Eqs. (13) and (14) because $d\psi_n/dt = 0$ for the stationary solution. This is confirmed in Eq. (5) explicitly for the limit ($\lambda = -1$) of the isolated edge states, and numerically for any value of λ .

We show the saturated amplitude $|\psi_1|$ as a function of the dimerization λ in Fig. 3(a1). It is finite for the topological phase although it deviates from 1 other than $\lambda = -1$ due to the hopping term. On the other hand, it is almost zero for the trivial phase. These features correspond to the emergence or the absence of the topological edge states as shown in Fig. 3(a2). Namely, the quench dynamics well signatures the topological phase transition although there are nonlinear non-Hermitian terms.

We also study the dynamics under the initial condition (11) by taking the site m in the bulk. The result is shown in Fig. 5 by choosing $m = 7$. All sites belonging to the two topological edge states are stimulated after a delay with the intensity depending on the DOS. The timing of the stimulation is determined by the distance from the initial site.

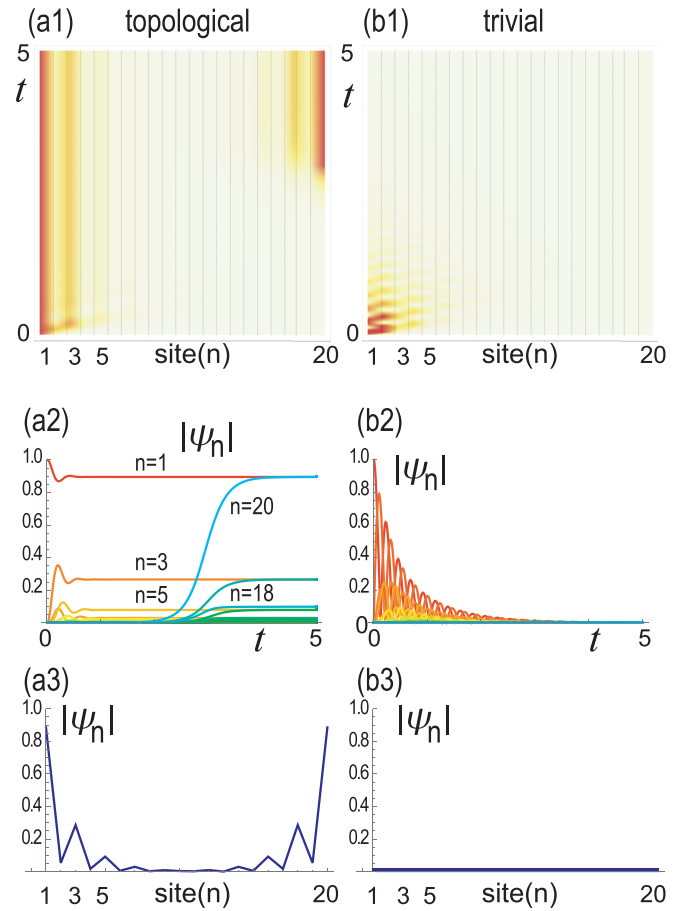


FIG. 4. Density plot of the time evolution of the amplitude $|\psi_n|$ as a function of n in (a1) the topological phase with $\lambda = -0.5$ and (b1) the trivial phase with $\lambda = 0.5$ in the SSH model. The amplitude $|\psi_n|$ as a function of t for various n in (a2) the topological phase and (b2) the trivial phase, where red curves indicate $n = 1$, while cyan curves indicate $n = N$ in (a2) and (b2). The saturated amplitude $|\psi_n|$ as a function of n in (a3) the topological phase and (b3) the trivial phase after enough time. We have set $\kappa = 1$, $\eta = 1$, $\gamma = 1/2$, and $\xi = 2$. We take a sample with $N = 20$.

It is possible to control the time delay by tuning the hopping amplitude κ . We have studied the dependence of the time evolution of lasing on κ . The starting time of illumination gets faster (later) for larger (smaller) κ as shown in Figs. 6(a) and 6(b). We exhibit the time evolution of $|\psi_L|$ in Fig. 6(c) for various κ , which also proves that the time delay is controlled by tuning κ .

D. Dimer states

We study the trivial phase ($\lambda > 1$). In particular, we may solve the equations of motion analytically in the dimer limit ($\lambda = 1$). In this case, we obtain a closed set of equations for sites 1 and 2,

$$i \frac{d\psi_1}{dt} = \kappa_A(\psi_2 - \psi_1) - i\gamma \left(1 - \xi \frac{1}{1 + |\psi_1|^2/\eta} \right) \psi_1, \quad (22)$$

$$i \frac{d\psi_2}{dt} = \kappa_A(\psi_1 - \psi_2). \quad (23)$$

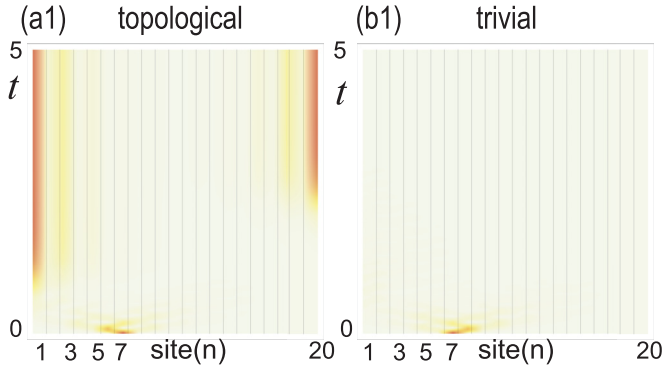


FIG. 5. Density plot of the time evolution of the amplitude $|\psi_n|$ as a function of n in (a1) the topological phase with $\lambda = -0.5$ and (b1) the trivial phase with $\lambda = 0.5$ in the SSH model. We start from the site $n = 7$. We have set $\kappa = 1$, $\eta = 1$, $\gamma = 1/2$, and $\xi = 2$. We take a sample with $N = 20$.

The stationary solutions of (22) and (23) are either the trivial one

$$\psi_1 = \psi_2 = 0, \quad (24)$$

or a nontrivial one

$$\psi_1 = \sqrt{\eta(\xi - 1)}, \quad \psi_2 = \text{const}. \quad (25)$$

We note that it is not necessary for the right-hand side of Eq. (23) to be zero because only the phase rotates if it is not zero. Which stationary solution is actually chosen is a dynamical problem depending on the initial condition.

We show the numerical solution with the initial condition $\psi_1 = 1$ and $\psi_2 = 0$ in Fig. 7(a). The amplitudes $|\psi_1|$ and $|\psi_2|$ exponentially decrease to zero with oscillations. Hence the stationary solutions are $\psi_1 = \psi_2 = 0$. Furthermore, we have found numerically that $|\psi_1|$ is almost zero in the trivial phase as in Fig. 3(a1). As far as we have checked numerically, there is no nontrivial dimer solution in the trivial phase of the SSH model.

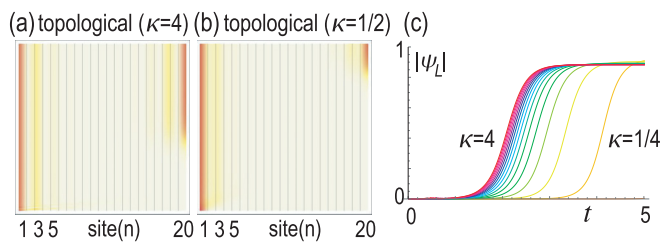


FIG. 6. Control of the delay time. Density plot of the time evolution of the amplitude $|\psi_n|$ as a function of n with (a) $\kappa = 4$ and (b) $\kappa = 1/2$, and the time evolution of the laser intensity $|\psi_L|$ with (c) $\kappa = p/4$, where $p = 1, 2, \dots, 16$. In (c), the vertical axis is the laser intensity $|\psi_L|$, and the horizontal axis is the time t . The parameters are the same as in Fig. 3.

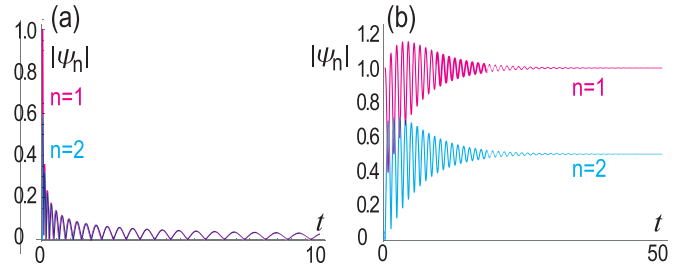


FIG. 7. (a) Dynamics of the amplitude $|\psi_n|$ of the dimer in the SSH model (22) and (23). (b) Dynamics of the trimer in the breathing kagome model (35) and (36). We have set $\kappa_A = 1$, $\eta = 1$, $\gamma = 1/2$, and $\xi = 2$.

IV. NONLINEAR NON-HERMITIAN BREATHING KAGOME MODEL

A. Model

We proceed to investigate the system where the hopping matrix M_{nm} describes the breathing kagome lattice, whose lattice structure is illustrated in Figs. 1(b1)–1(b3). The hopping matrix is explicitly given by [62]

$$M(\mathbf{k}) = - \begin{pmatrix} 0 & h_{12} & h_{13} \\ h_{12}^* & 0 & h_{23} \\ h_{13}^* & h_{23}^* & 0 \end{pmatrix} \quad (26)$$

with

$$h_{12} = \kappa_A e^{i(k_x/2 + \sqrt{3}k_y/2)} + \kappa_B e^{-i(k_x/2 + \sqrt{3}k_y/2)}, \quad (27)$$

$$h_{23} = \kappa_A e^{i(k_x/2 - \sqrt{3}k_y/2)} + \kappa_B e^{i(-k_x/2 + \sqrt{3}k_y/2)}, \quad (28)$$

$$h_{13} = \kappa_A e^{ik_x} + \kappa_B e^{-ik_x} \quad (29)$$

in the momentum space, where we have introduced two hopping parameters κ_A and κ_B corresponding to the upward and downward triangles in Figs. 1(b1)–1(b3).

B. Topological number in the breathing kagome model

The topological number in the breathing kagome model is defined by [62]

$$\Gamma = 3(p_x^2 + p_y^2), \quad (30)$$

where

$$p_i = \frac{1}{S} \int_{\text{BZ}} A_i d^2\mathbf{k}, \quad (31)$$

with $A_i = -i\langle\phi(\mathbf{k})|\partial_{k_i}|\phi(\mathbf{k})\rangle$ being the Berry connection with $x_i = x, y$, and $S = 8\pi^2/\sqrt{3}$ being the area of the Brillouin zone (BZ); $\phi(\mathbf{k})$ is the eigenfunction of $M(\mathbf{k})$. We obtain $\Gamma = 0$ for $1 \geq \lambda > 1/3$, which is the trivial phase with no topological corner states. On the other hand, we obtain $\Gamma = 1$ for $-1 \leq \lambda < -1/3$, which is the topological phase with the emergence of three topological corner states. Finally, Γ is not quantized for $-1/3 < \lambda < 1/3$, which is the metal phase. See Fig. 3(b2).

C. Quench dynamics

By solving Eq. (1) under the initial condition (11) with the choice of $m = 1$, we show the time evolution of the amplitude

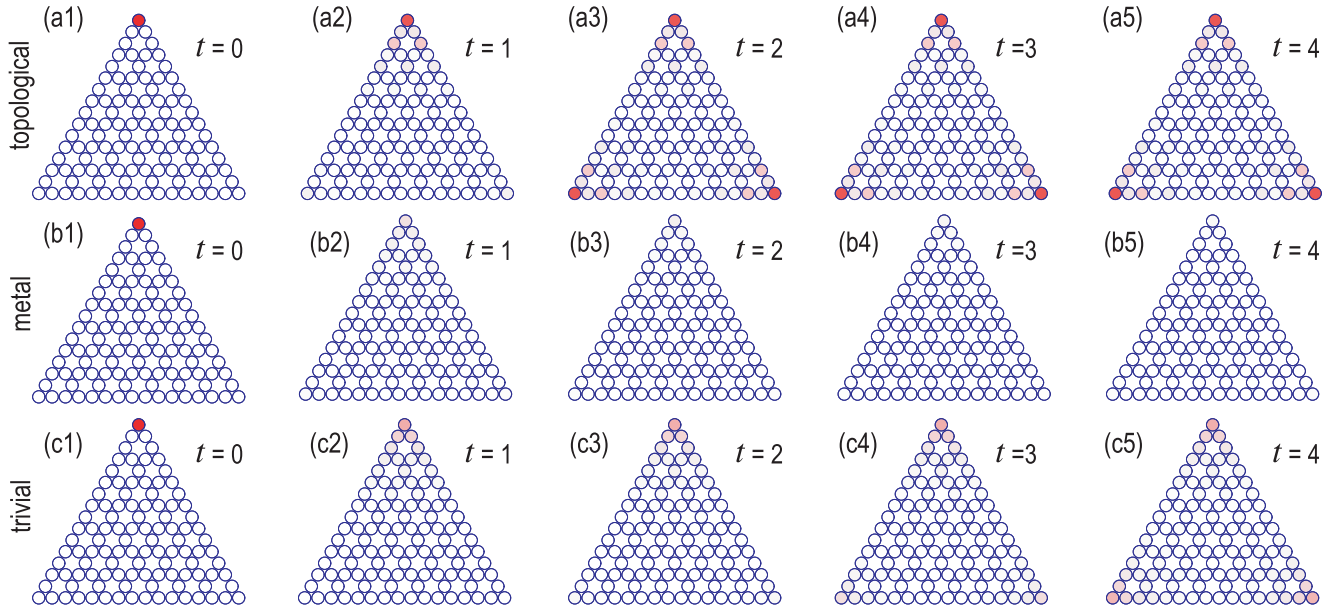


FIG. 8. Time evolution of the amplitude $|\psi_n|$ of the breathing kagome model in (a1)–(a5) the topological phase with $\lambda = -0.5$, (b1)–(b5) the metal phase with $\lambda = 0.2$, and (c1)–(c5) the trivial phase with $\lambda = 0.5$. The color density indicates the amplitude $|\psi_n|$. (a5) and (c5) give the profiles of the topological corner states and the trimer states together with their DOS, respectively. We have set $\kappa = 1$, $\eta = 1$, $\gamma = 1/2$, and $\xi = 2$. We take a triangle with $N = 108$.

$|\psi_n|$ in Figs. 8 and 9, where $n = 1$ denotes the top-corner site. Figure 8 displays a global picture of how the stimulated signal at site $n = 1$ propagates all over the sites as time evolves. Figure 9 displays a detailed evolution along the left side of the lattice. We also show the saturated amplitude as a function of λ in Fig. 3(b1). The saturated amplitudes are identical at the three corner sites due to trigonal symmetry of the breathing kagome lattice, as found in Fig. 8.

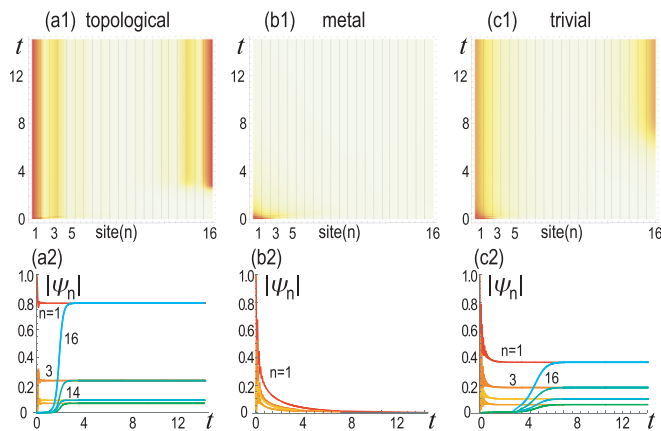


FIG. 9. Density plot of the time evolution of the amplitude $|\psi_n|$ along one side of the breathing kagome lattice in the (a1) topological phase with $\lambda = -0.5$, (b1) metal phase with $\lambda = 0.2$, and (c1) trivial phase with $\lambda = 0.5$. Time evolution of the amplitude $|\psi_n|$ of the breathing kagome model for various n in the (a2) topological phase with $\lambda = -0.5$, (b2) metal phase with $\lambda = 0.2$, and (c2) trivial phase with $\lambda = 0.5$. We have set $\kappa = 1$, $\eta = 1$, $\gamma = 1/2$, and $\xi = 2$. We take a triangle with $N = 108$.

We comment that Fig. 8(a5) shows a spatial profile of the saturated amplitude $|\psi_n|$, which is the DOS for three topological corner states in a nonlinear non-Hermitian system.

These figures show typically different behaviors in the topological, trivial, and metal phases. First, in the topological phase, the amplitudes at the other two corner sites increase after a delay to the saturated amplitude as shown in Fig. 9(a2). Second, in the metal phase, the amplitude at the corner site rapidly decreases as in Fig. 9(b2). These features are very much similar to those in the the SSH model.

On the other hand, in the trivial phase, there is a significant difference between the SSH model and the breathing kagome model. In the SSH model, the amplitude rapidly decreases as in Fig. 4(b2). However, this is not the case for the breathing kagome model. The amplitude at the top corner site suddenly decreases to the saturated value, while those at the bottom corner sites increase to the saturated value after a delay as in Fig. 9(c2). Furthermore, the saturated amplitude $|\psi_1|$ depends on the magnitude of ξ as shown in Fig. 3(b1). We pursue the reason why the amplitudes do not vanish in the trivial phase. We will see that it is due to the formation of the trimer state.

D. Trimer states

We consider the limit $\lambda = 1$, where the system is decomposed into a set of trimers as in Fig. 1(b3). The equations of motion are explicitly given by

$$i \frac{d\psi_1}{dt} = \kappa_A(\psi_2 + \psi_3) - i\gamma \left(1 - \xi \frac{1}{1 + |\psi_1|^2/\eta} \right) \psi_1, \quad (32)$$

$$i \frac{d\psi_2}{dt} = \kappa_A(\psi_1 + \psi_3), \quad (33)$$

$$i \frac{d\psi_3}{dt} = \kappa_A(\psi_1 + \psi_2). \quad (34)$$

Without loss of generality we may set $\psi_2 = \psi_3$ and obtain

$$i\frac{d\psi_1}{dt} = 2\kappa_A\psi_2 - i\gamma\left(1 - \xi\frac{1}{1 + |\psi_1|^2/\eta}\right)\psi_1, \quad (35)$$

$$i\frac{d\psi_2}{dt} = \kappa_A(\psi_1 + \psi_2). \quad (36)$$

The stationary solutions are either the trivial one

$$\psi_1 = \psi_2 = 0, \quad (37)$$

or a nontrivial one

$$\psi_1 = \sqrt{\eta(\xi - 1)}, \quad \psi_2 = \text{const}, \quad (38)$$

which is identical to the stationary solution (25) in the SSH model. There is no γ dependence in the stationary solution (38), which agrees with the results shown in Fig. 3(b1).

We have found analytically the trimer state in the limit of $\lambda = 1$ in the trivial phase. A numerical solution is given as a function of time t in Fig. 7(b), where $|\psi_1|$ and $|\psi_2|$ approach two saturated values (38), as is consistent with Fig. 3(b1). Figure 3(b1) suggests that the trimer state is formed also away from the limit $\lambda = 1$ depending on the value of γ . Indeed, Fig. 8(c5) shows a spatial profile of three trimer states at $\lambda = 0.5$. The formation of trimer states implies the presence of a nontopological laser in the breathing kagome model. These behaviors are contrasted with the dimer state in the SSH model, where $|\psi_1| = 0$ in the trivial phase as in Fig. 3(a1).

V. DISCUSSION

A topological laser provides a unique arena of topology, non-Hermiticity, and nonlinearity. We have studied topological lasing in the SSH lattice and the breathing kagome lattice. They have topological edge or corner states in the topological phase. When any one site is stimulated, all sites belonging to the topological edge or corner states begin to emit stable laser light depending on the DOS. The results would be universal for the physics of topological lasing with the use of topological edge or corner states.

Non-Hermiticity and nonlinearity play essential roles in the stabilization of lasing. Without the nonlinearity, there is

no stable lasing because the amplitude exponentially grows or decays. The amplifier plays an essential role in the lasing. If there is no loss term, there should be a reflection wave at the right-edge site or the bottom-corner sites, which is absent in a topological laser.

On the other hand, nontopological lasing is not universal. Indeed, the quench dynamics is different between the SSH model and the breathing kagome model in the trivial phase. There is no stable laser emission in the SSH model. However, once one site is stimulated, all three corner states emit stable laser lights in the breathing kagome model due to the formation of trimer states at the three corners.

Topological lasing has already been experimentally realized based on models such as the SSH model [12,18,50–53] and a Chern insulator [47]. It must be possible to realize the present model experimentally using the existing technique.

Comments are in order. First, there are various studies on Hermitian nonlinear topological physics, although they are not directly related to topological lasing. A nonlinear SSH model was theoretically proposed [69] and then experimentally investigated [70], where the linear and nonlinear bonds are alternating. The nonlinear term is introduced by a back-to-back varactor in electric circuits [70]. Second, higher-order topological physics has already been studied in the context of Hermitian nonlinear photonics [71,72].

In conclusion, we have found stable laser emission to occur in the topological phase. Our results show that topological lasers provide an ideal playground of nonlinear non-Hermitian topological physics, where a topological edge or corner state is observable by measuring the real space-time dynamics of lasing.

ACKNOWLEDGMENTS

The author is very much grateful to S. Iwamoto and N. Nagaosa for helpful discussions on this subject. This work is supported by the Grants-in-Aid for Scientific Research from MEXT KAKENHI (Grants No. JP17K05490 and No. JP18H03676). This work is also supported by CREST, JST (Grants No. JPMJCR16F1 and No. JPMJCR20T2).

-
- [1] M. Z. Hasan and C. L. Kane, *Colloquium: Topological insulators*, *Rev. Mod. Phys.* **82**, 3045 (2010).
 - [2] X.-L. Qi and S.-C. Zhang, *Topological insulators and superconductors*, *Rev. Mod. Phys.* **83**, 1057 (2011).
 - [3] A. B. Khanikaev, S. H. Mousavi, W.-K. Tse, M. Kargarian, A. H. MacDonald, and G. Shvets, *Photonic topological insulators*, *Nat. Mater.* **12**, 233 (2013).
 - [4] M. Hafezi, E. Demler, M. Lukin, and J. Taylor, *Robust optical delay lines with topological protection*, *Nat. Phys.* **7**, 907 (2011).
 - [5] M. Hafezi, S. Mittal, J. Fan, A. Migdall, and J. Taylor, *Imaging topological edge states in silicon photonics*, *Nat. Photonics* **7**, 1001 (2013).
 - [6] L. H. Wu and X. Hu, *Scheme for Achieving a Topological Photonic Crystal by Using Dielectric Material*, *Phys. Rev. Lett.* **114**, 223901 (2015).
 - [7] L. Lu, J. D. Joannopoulos, and M. Soljacic, *Topological photonics*, *Nat. Photonics* **8**, 821 (2014).
 - [8] T. Ozawa, H. M. Price, N. Goldman, O. Zilberberg, and I. Carusotto, *Synthetic dimensions in integrated photonics: From optical isolation to four-dimensional quantum Hall physics*, *Phys. Rev. A* **93**, 043827 (2016).
 - [9] D. Leykam and Y. D. Chong, *Edge Solitons in Nonlinear-Photonic Topological Insulators*, *Phys. Rev. Lett.* **117**, 143901 (2016).
 - [10] A. B. Khanikaev and G. Shvets, *Two-dimensional topological photonics*, *Nat. Photonics* **11**, 763 (2017).
 - [11] X. Zhou, Y. Wang, D. Leykam, and Y. D. Chong, *Optical isolation with nonlinear topological photonics*, *New J. Phys.* **19**, 095002 (2017).
 - [12] P. St-Jean, V. Goblot, E. Galopin, A. Lemaitre, T. Ozawa, L. Le Gratiet, I. Sagnes, J. Bloch, and A. Amo, *Lasing in*

- topological edge states of a 1D lattice, *Nat. Photonics* **11**, 651 (2017).
- [13] Y. Ota, R. Katsumi, K. Watanabe, S. Iwamoto, and Y. Arakawa, Topological photonic crystal nanocavity laser, *Commun. Phys.* **1**, 86 (2018).
- [14] T. Ozawa, H. M. Price, A. Amo, N. Goldman, M. Hafezi, L. Lu, M. C. Rechtsman, D. Schuster, J. Simon, O. Zilberberg, and I. Carusotto, Topological photonics, *Rev. Mod. Phys.* **91**, 015006 (2019).
- [15] Y. Ota, F. Liu, R. Katsumi, K. Watanabe, K. Wakabayashi, Y. Arakawa, and S. Iwamoto, Photonic crystal nanocavity based on a topological corner state, *Optica* **6**, 786 (2019).
- [16] T. Ozawa and H. M. Price, Topological quantum matter in synthetic dimensions, *Nat. Rev. Phys.* **1**, 349 (2019).
- [17] A. E. Hassan, F. K. Kunst, A. Moritz, G. Andler, E. J. Bergholtz, and M. Bourennane, Corner states of light in photonic waveguides, *Nat. Photonics* **13**, 697 (2019).
- [18] Y. Ota, K. Takata, T. Ozawa, A. Amo, Z. Jia, B. Kante, M. Notomi, Y. Arakawa, and S. Iwamoto, Active topological photonics, *Nanophotonics* **9**, 547 (2020).
- [19] M. Li, D. Zhirihin, D. Filonov, X. Ni, A. Slobozhanyuk, A. Alu, and A. B. Khanikaev, Higher-order topological states in photonic kagome crystals with long-range interactions, *Nat. Photonics* **14**, 89 (2020).
- [20] H. Yoshimi, T. Yamaguchi, Y. Ota, Y. Arakawa, and S. Iwamoto, Slow light waveguides in topological valley photonic crystals, *Opt. Lett.* **45**, 2648 (2020).
- [21] M. Kim, Z. Jacob, and J. Rho, Recent advances in 2D, 3D and higher-order topological photonics, *Light: Sci. Appl.* **9**, 130 (2020).
- [22] S. Iwamoto, Y. Ota, and Y. Arakawa, Recent progress in topological waveguides and nanocavities in a semiconductor photonic crystal platform, *Opt. Mater. Express* **11**, 319 (2021).
- [23] E. Prodan and C. Prodan, Topological Phonon Modes and Their Role in Dynamic Instability of Microtubules, *Phys. Rev. Lett.* **103**, 248101 (2009).
- [24] Z. Yang, F. Gao, X. Shi, X. Lin, Z. Gao, Y. Chong, and B. Zhang, Topological Acoustics, *Phys. Rev. Lett.* **114**, 114301 (2015).
- [25] P. Wang, L. Lu, and K. Bertoldi, Topological Phononic Crystals with One-Way Elastic Edge Waves, *Phys. Rev. Lett.* **115**, 104302 (2015).
- [26] M. Xiao, G. Ma, Z. Yang, P. Sheng, Z. Q. Zhang, and C. T. Chan, Geometric phase and band inversion in periodic acoustic systems, *Nat. Phys.* **11**, 240 (2015).
- [27] C. He, X. Ni, H. Ge, X.-C. Sun, Y.-B. Chen, M.-H. Lu, X.-P. Liu, L. Feng, and Y.-F. Chen, Acoustic topological insulator and robust one-way sound transport, *Nat. Phys.* **12**, 1124 (2016).
- [28] H. Abbaszadeh, A. Souslov, J. Paulose, H. Schomerus, and V. Vitelli, Sonic Landau Levels and Synthetic Gauge Fields in Mechanical Metamaterials, *Phys. Rev. Lett.* **119**, 195502 (2017).
- [29] H. Xue, Y. Yang, F. Gao, Y. Chong, and B. Zhang, Acoustic higher-order topological insulator on a kagome lattice, *Nat. Mater.* **18**, 108 (2019).
- [30] X. Ni, M. Weiner, A. Alu, and A. B. Khanikaev, Observation of higher-order topological acoustic states protected by generalized chiral symmetry, *Nat. Mater.* **18**, 113 (2019).
- [31] M. Weiner, X. Ni, M. Li, A. Alu, and A. B. Khanikaev, Demonstration of a third-order hierarchy of topological states in a three-dimensional acoustic metamaterial, *Sci. Adv.* **6**, eaay4166 (2020).
- [32] H. Xue, Y. Yang, G. Liu, F. Gao, Y. Chong, and B. Zhang, Realization of an Acoustic Third-Order Topological Insulator, *Phys. Rev. Lett.* **122**, 244301 (2019).
- [33] C. L. Kane and T. C. Lubensky, Topological boundary modes in isostatic lattices, *Nat. Phys.* **10**, 39 (2014).
- [34] B. G.-g. Chen, N. Upadhyaya, and V. Vitelli, Nonlinear conduction via solitons in a topological mechanical insulator, *Proc. Natl. Acad. Sci. USA* **111**, 13004 (2014).
- [35] L. M. Nash, D. Kleckner, A. Read, V. Vitelli, A. M. Turner, and W. T. M. Irvine, Topological mechanics of gyroscopic metamaterials, *Proc. Natl. Acad. Sci. USA* **112**, 14495 (2015).
- [36] J. Paulose, A. S. Meeussen, and V. Vitelli, Selective buckling via states of self-stress in topological metamaterials, *Proc. Natl. Acad. Sci. USA* **112**, 7639 (2015).
- [37] R. Susstrunk and S. D. Huber, Observation of phononic helical edge states in a mechanical topological insulator, *Science* **349**, 47 (2015).
- [38] S. Imhof, C. Berger, F. Bayer, J. Brehm, L. Molenkamp, T. Kiessling, F. Schindler, C. H. Lee, M. Greiter, T. Neupert, and R. Thomale, Topoelectrical-circuit realization of topological corner modes, *Nat. Phys.* **14**, 925 (2018).
- [39] C. H. Lee, S. Imhof, C. Berger, F. Bayer, J. Brehm, L. W. Molenkamp, T. Kiessling, and R. Thomale, Topoelectrical circuits, *Commun. Phys.* **1**, 39 (2018).
- [40] T. Helbig, T. Hofmann, C. H. Lee, R. Thomale, S. Imhof, L. W. Molenkamp, and T. Kiessling, Band structure engineering and reconstruction in electric circuit networks, *Phys. Rev. B* **99**, 161114(R) (2019).
- [41] Y. Lu, N. Jia, L. Su, C. Owens, G. Juzeliunas, D. I. Schuster, and J. Simon, Probing the Berry curvature and Fermi arcs of a Weyl circuit, *Phys. Rev. B* **99**, 020302(R) (2019).
- [42] Y. Li, Y. Sun, W. Zhu, Z. Guo, J. Jiang, T. Kariyado, H. Chen, and X. Hu, Topological LC-circuits based on microstrips and observation of electromagnetic modes with orbital angular momentum, *Nat. Commun.* **9**, 4598 (2018).
- [43] M. Ezawa, Higher-order topological electric circuits and topological corner resonance on the breathing kagome and pyrochlore lattices, *Phys. Rev. B* **98**, 201402(R) (2018).
- [44] M. Ezawa, Non-Hermitian higher-order topological states in nonreciprocal and reciprocal systems with their electric-circuit realization, *Phys. Rev. B* **99**, 201411(R) (2019).
- [45] M. Ezawa, Non-Hermitian boundary and interface states in nonreciprocal higher-order topological metals and electrical circuits, *Phys. Rev. B* **99**, 121411(R) (2019).
- [46] G. Harari, M. A. Bandres, Y. Lumer, M. C. Rechtsman, Y. D. Chong, M. Khajavikhan, D. N. Christodoulides, and M. Segev, Topological insulator laser: Theory, *Science* **359**, eaar4003 (2018).
- [47] M. A. Bandres, S. Wittek, G. Harari, M. Parto, J. Ren, M. Segev, D. N. Christodoulides, and M. Khajavikhan, Topological insulator laser: Experiments, *Science* **359**, 1231 (2018).
- [48] H. Schomerus, Topologically protected midgap states in complex photonic lattices, *Opt. Lett.* **38**, 1912 (2013).
- [49] S. Weimann, M. Kremer, Y. Plotnik, Y. Lumer, S. Nolte, K. G. Makris, M. Segev, M. C. Rechtsman, and A. Szameit, Topologically protected bound states in photonic parity-time-symmetric crystals, *Nat. Mater.* **16**, 433 (2017).

- [50] M. Parto, S. Wittek, H. Hodaei, G. Harari, M. A. Bandres, J. Ren, M. C. Rechtsman, M. Segev, D. N. Christodoulides, and M. Khajavikhan, Edge-Mode Lasing in 1D Topological Active Arrays, *Phys. Rev. Lett.* **120**, 113901 (2018).
- [51] H. Zhao, P. Miao, M. H. Teimourpour, S. Malzard, R. El-Ganainy, H. Schomerus, and L. Feng, Topological hybrid silicon microlasers, *Nat. Commun.* **9**, 981 (2018).
- [52] S. Malzard and H. Schomerus, Nonlinear mode competition and symmetry-protected power oscillations in topological lasers, *New J. Phys.* **20**, 063044 (2018).
- [53] S. Malzard, E. Cancellieri, and H. Schomerus, Topological dynamics and excitations in lasers and condensates with saturable gain or loss, *Opt. Express* **26**, 22506 (2018).
- [54] H. Zhong, Y. V. Kartashov, A. Szameit, Y. Li, C. Liu, and Y. Zhang, Theory of topological corner state laser in kagome waveguide arrays, *APL Photonics* **6**, 040802 (2021).
- [55] F. Zhang, C. L. Kane, and E. J. Mele, Surface State Magnetization and Chiral Edge States on Topological Insulators, *Phys. Rev. Lett.* **110**, 046404 (2013).
- [56] W. A. Benalcazar, B. A. Bernevig, and T. L. Hughes, Quantized electric multipole insulators, *Science* **357**, 61 (2017).
- [57] Y. Peng, Y. Bao, and F. von Oppen, Boundary Green functions of topological insulators and superconductors, *Phys. Rev. B* **95**, 235143 (2017).
- [58] J. Langbehn, Y. Peng, L. Trifunovic, F. von Oppen, and P. W. Brouwer, Reflection-Symmetric Second-Order Topological Insulators and Superconductors, *Phys. Rev. Lett.* **119**, 246401 (2017).
- [59] Z. Song, Z. Fang, and C. Fang, $(d - 2)$ -Dimensional Edge States of Rotation Symmetry Protected Topological States, *Phys. Rev. Lett.* **119**, 246402 (2017).
- [60] W. A. Benalcazar, B. A. Bernevig, and T. L. Hughes, Electric multipole moments, topological multipole moment pumping, and chiral hinge states in crystalline insulators, *Phys. Rev. B* **96**, 245115 (2017).
- [61] F. Schindler, A. M. Cook, M. G. Vergniory, Z. Wang, S. S. P. Parkin, B. A. Bernevig, and T. Neupert, Higher-order topological insulators, *Sci. Adv.* **4**, eaat0346 (2018).
- [62] M. Ezawa, Higher-Order Topological Insulators and Semimetals on the Breathing Kagome and Pyrochlore Lattices, *Phys. Rev. Lett.* **120**, 026801 (2018).
- [63] J. Wu, X. Huang, J. Lu, Y. Wu, W. Deng, F. Li, and Z. Liu, Observation of corner states in second-order topological electric circuits, *Phys. Rev. B* **102**, 104109 (2020).
- [64] M. Ezawa, Electric-circuit simulation of the Schrödinger equation and non-Hermitian quantum walks, *Phys. Rev. B* **100**, 165419 (2019).
- [65] M. Ezawa, Topological edge states and bulk-edge correspondence in dimerized Toda lattice, *J. Phys. Soc. Jpn.* **91**, 024703 (2022).
- [66] M. Ezawa, Quench dynamics and bulk-edge correspondence in nonlinear mechanical systems, *J. Phys. Soc. Jpn.* **90**, 114605 (2021).
- [67] M. Ezawa, Nonlinearity-induced transition in nonlinear Su-Schrieffer-Heeger model and a nonlinear higher-order topological system, *Phys. Rev. B* **104**, 235420 (2021).
- [68] M. Ezawa, Nonlinear topological phase diagram in dimerized Sine-Gordon model, [arXiv:2110.15602](https://arxiv.org/abs/2110.15602) [cond-mat.mes-hall].
- [69] Y. Hadad, A. B. Khanikaev, and A. Alu, Self-induced topological transitions and edge states supported by nonlinear staggered potentials, *Phys. Rev. B* **93**, 155112 (2016).
- [70] Y. Hadad, J. C. Soric, A. B. Khanikaev, and A. Alu, Self-induced topological protection in nonlinear circuit arrays, *Nat. Electron.* **1**, 178 (2018).
- [71] G. D'Aguanno, Y. Hadad, D. A. Smirnova, X. Ni, A. B. Khanikaev, and A. Alù, Nonlinear topological transitions over a metasurface, *Phys. Rev. B* **100**, 214310 (2019).
- [72] M. S. Kirsch, Y. Zhang, M. Kremer, L. J. Maczewsky, S. K. Ivanov, Y. V. Kartashov, L. Torner, D. Bauer, A. Szameit, and M. Heinrich, Nonlinear second-order photonic topological insulators, *Nat. Phys.* **17**, 995 (2021).